

Near Real-Time Mapping of Peak Ground Acceleration and Peak Ground Velocity Following a Strong Earthquake

by Yih-Min Wu, Tzay-Chyn Shin, and Chien-Hsin Chang

Abstract During a disastrous earthquake, the early assessment and timely reporting of the peak ground acceleration (PGA) and peak ground velocity (PGV) maps will be crucial in an effective emergency response operation. In this study, we first derive an empirical relationship between M_L and M_W . The PGA and PGV attenuation relationships are deduced with data from the Taiwan Strong Motion Instrumentation Program (TSMIP) and the Taiwan Rapid Earthquake Information Release System (TREIRS). Site corrections of the attenuation relationships for shallow and large earthquakes in Taiwan region are also obtained. Peak values of earthquake strong ground motion can be well determined in Taiwan as soon as the earthquake location is determined, and magnitudes are calculated by the TREIRS. This peak ground motion value information can be immediately turned into the calculated PGA and PGV maps that can be issued within two minutes of the earthquake origin time. During any disastrous earthquake, these maps are found to be very useful for immediate seismic damage assessment and dispatching of emergency response missions.

Introduction

Real-time seismic monitoring, especially for strong earthquakes, is an important tool for seismic hazard mitigation (Kanamori *et al.*, 1997; Teng *et al.*, 1997). It provides valuable near-real-time information for rapid earthquake emergency response, thereby mitigating the loss. With the importance of rapid earthquake information for seismic hazard mitigation being recognized, efforts to design and implement systems to provide a broad range of rapid earthquake information have recently been expanded (Heaton, 1985; Nakamura, 1988, 1989; Espinosa-Aranda, *et al.*, 1995; Gee *et al.*, 1996; Wu *et al.*, 1997, 1998, 1999; Wald *et al.*, 1999a,b). During the 1999 Chi-Chi, Taiwan, earthquake a severe test was put on the Taiwan Rapid Earthquake Information Release System (TREIRS) system (Shin *et al.*, 2000; Wu *et al.*, 2000). For the purpose of brevity, we use the term *T system* to mean the TREIRS in this article. We also report our experience and thoughts in the development and application of the T system.

The most common information available immediately following a damaging earthquake is its magnitude and epicenter. However, the damage pattern is not a simple function of these two parameters alone. More detailed information is needed for emergency response agencies to assess the situation for better details and accuracy. For example, for the 20 September 1999 Chi-Chi, Taiwan, earthquake, the city of Tung-Shih Town is in the region with the worst damage, even though it is about 50 km from the epicenter (Fig. 1). Thus, it is highly desirable to map out distributions of peak

ground acceleration (PGA) and peak ground velocity (PGV) in the potentially damaged area. In 1995, the Central Weather Bureau (CWB) developed the T system by a real-time strong-motion network for intensity observations, magnitude, and hypocenter determination routinely after felt earthquakes in the Taiwan region (Teng *et al.*, 1997; Wu *et al.*, 1997).

The T system consists of 75 telemetered strong-motion stations in Taiwan (Fig. 2). Three-component force-balanced accelerometer (FBA) digital signals are continuously telemetered to the headquarters of the CWB in Taipei via leased telephone lines. The FBA signal is digitized at 50 samples per sec at a 16-bit resolution. The full recording range is $\pm 2g$. The interstation spacing of the T system is about 30 km. This spacing is still too large for the damage assessment due to complex geology in Taiwan (Lee *et al.*, 2001). On the other hand, the Taiwan Strong Motion Instrumentation Program (TSMIP) was successfully implemented six years ago by the CWB, with about 650 modern digital accelerographs at free-field sites (Fig. 2). The TSMIP signals are digitized at 200 samples per sec or higher and at 16-bit or higher resolution. Most accelerometer sensor recording ranges are $\pm 2g$. The TSMIP interstation spacing is about 5 km in metropolitan areas. It offers much more detailed description of ground shaking for damage assessment. But they are not continuously telemetered. In this study we combine the data from the T system and the TSMIP network to determine the site corrections. Then, the database of TSMIP site corrections

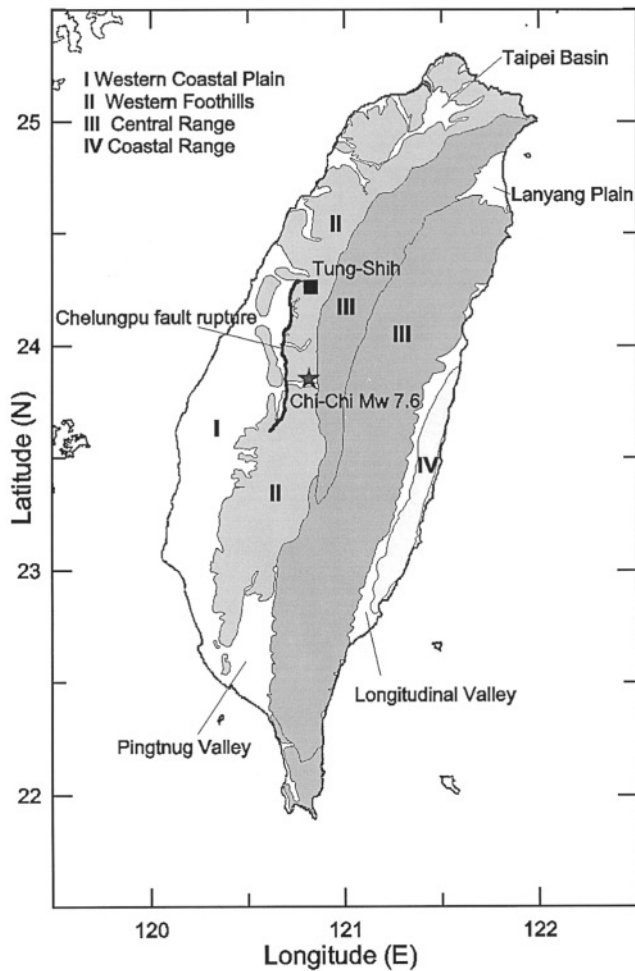


Figure 1. The Chi-Chi mainshock epicenter, the Chelungpu fault rupture, and topographical settings of Taiwan.

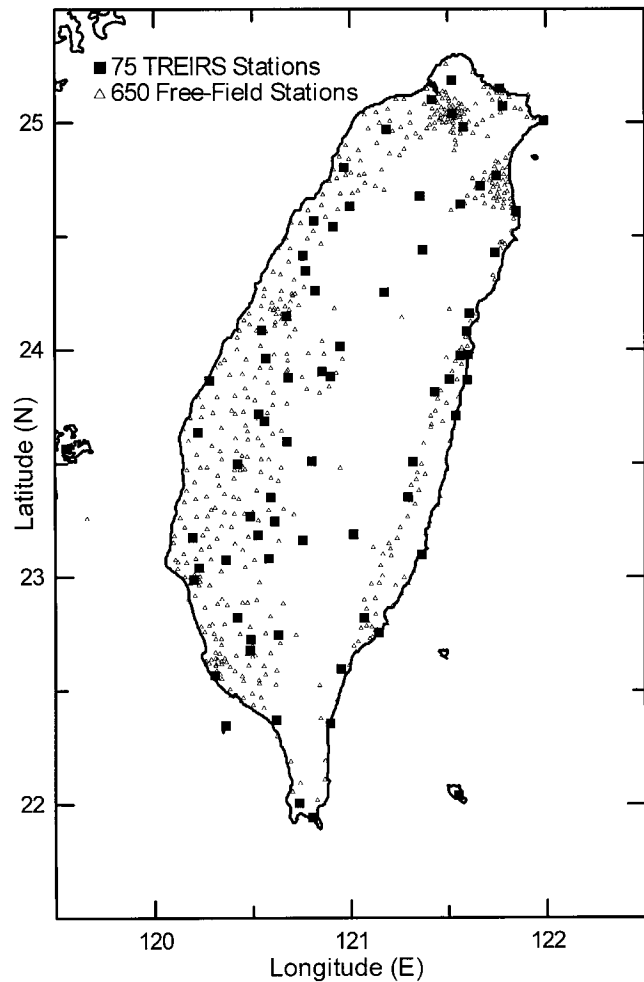


Figure 2. Distribution of the 75 TREIRS stations and the 650 TSMIP stations.

will be integrated into the T system to estimate the PGA and PGV values at the TSMIP sites for the new earthquake. We are aiming at the issuance of these estimated peak values of ground motion within 2 min of the occurrence of a strong earthquake in Taiwan region.

Data

Big and shallow earthquakes often cause serious damage in heavily populated areas. Thus, we selected 60 large and shallow events in Taiwan for this study (Fig. 3 and Table 1). The selection criteria are M_L greater than 5.0 and focal depth less than 35 km. All events were well recorded by both the T system and TSMIP network. These events occurred in 1995 to 1999 and were widely felt in Taiwan. These earthquakes are relocated in this study by using both the T system and the TSMIP records. A total of 1369 T system records and 8262 TSMIP records are used for this study.

Relationship of the M_L and M_W for Shallow Earthquakes in Taiwan

We first use the T system accelerograms to simulate the Wood-Anderson seismograms from which we determine the local magnitude M_L (Shin, 1993). In our data set, 32 events have M_W reported by Harvard University Seismology Center. Therefore we use those 32 events to find the relationship between M_L and M_W and use this relationship to convert M_L to M_W for the following analysis. Figure 4 shows that M_L and M_W are correlated reasonably well, even though the number of data points for large events is limited and considering M_L is saturated in the large magnitude portion. Thus, M_L and $\ln(M_W)$ are used in the regression process. The empirical equation of the corresponding least-squares line is

$$M_L = 4.53 \times \ln(M_W) - 2.09 \pm 0.14, \quad (1)$$

for $5.0 \leq M_L \leq 7.1$ or $4.8 \leq M_W \leq 7.6$.

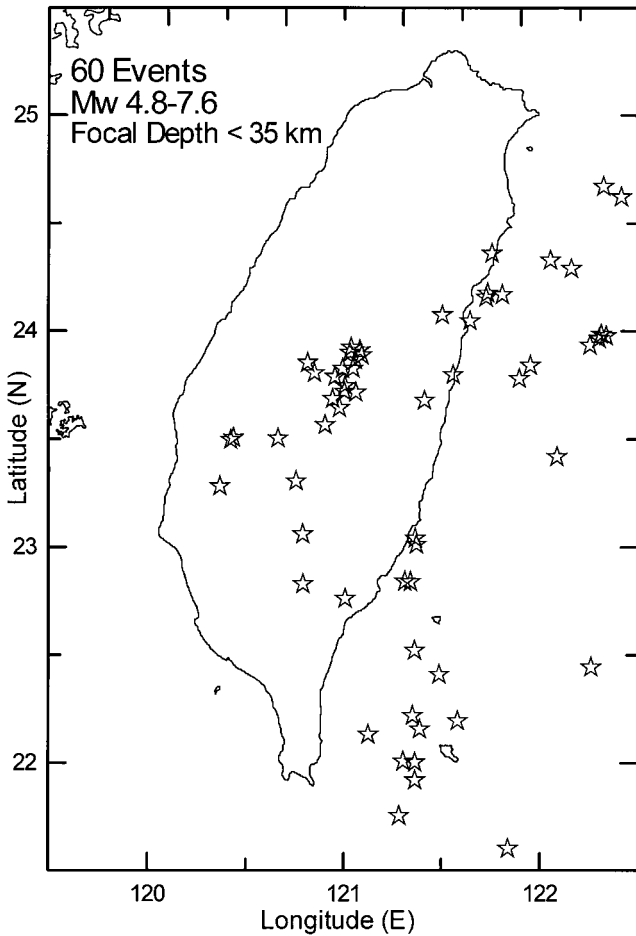


Figure 3. Epicentral distribution of the 60 events used in this study.

It is apparent that for $4.8 \leq M_W \leq 5.5$, the M_L is overestimated by about 0.2 unit; for $5.5 \leq M_W \leq 6.5$, the M_L is close to M_W . It is clear that M_L begins to saturate at about magnitude 6.5.

Attenuation Relationships for PGA and PGV

The Chi-Chi earthquake sequence is very energetic and provides a wealth of the digital data for large- and near-source observations. We used those data to determine the attenuation relationships for PGA and PGV. The basic linear regression model used is as following (Liu, 1999):

$$\log_{10}(Y) = C_1 + C_2 M_W - \log_{10}(r_{\text{rup}} + h) + C_3 r_{\text{rup}}, \quad (2)$$

where Y is either PGA or PGV, and r_{rup} is the source-to-site distance in terms of the closest distance to the rupture surface. If the surface was not defined for an event, then epicentral distance was used as the source-to-site distance. The variable h is the saturation term of the PGA and PGV for near-source observation. Here we use square root of rupture area for h . The coefficients C_1 , C_2 , and C_3 are to be deter-

Table 1
Earthquake Recordings Used in This Study.

Origin Time (UTC)		Lat. (N)	Long. (E)	Depth (km)	M_L (This Study)	M_W (Harvard)
Date (yy/mm/dd)	Time (hr:min:sec)					
95/01/10	07:55:19.71	23.677	121.412	11.25	5.18	5.1
95/02/10	02:21:59.78	23.779	121.894	20.24	5.03	-
95/02/23	05:19:01.79	24.169	121.807	22.03	6.27	6.2
95/04/03	11:54:40.09	23.977	122.334	5.00	5.79	5.6
95/05/02	22:48:20.71	23.840	121.950	22.96	5.31	-
95/05/09	01:03:51.37	23.012	121.373	22.22	5.03	-
95/05/27	18:11:11.92	23.040	121.367	21.98	5.60	5.7
95/06/28	14:14:53.64	22.220	121.354	6.87	5.20	5.3
95/07/07	03:04:48.45	23.888	121.092	13.57	5.45	-
95/07/14	16:52:46.93	24.361	121.754	9.29	5.57	-
95/10/14	03:01:36.86	24.622	122.409	5.00	5.04	-
95/10/31	22:27:06.61	23.281	120.368	18.07	5.10	-
95/12/18	16:17:54.49	24.047	121.643	29.48	5.39	5.2
95/12/25	19:05:28.23	22.838	121.343	5.00	5.19	-
96/03/05	14:52:27.98	23.964	122.298	8.87	6.24	6.3
96/03/05	17:32:08.10	23.934	122.252	5.00	5.93	5.8
96/03/29	03:28:52.91	23.985	122.309	2.38	5.72	5.7
96/05/28	21:53:23.10	24.075	121.502	19.89	5.23	-
96/07/27	00:26:39.51	24.329	122.051	10.13	5.02	-
96/08/10	06:23:05.70	23.885	122.649	5.57	5.81	5.6
96/09/05	23:42:07.73	22.003	121.366	9.92	6.49	6.8
96/09/06	02:04:56.39	21.920	121.366	7.98	5.53	-
96/09/06	11:34:32.06	21.754	121.285	5.00	5.37	5.4
96/11/14	01:39:11.24	23.418	122.086	12.80	5.16	-
96/12/18	11:20:23.77	22.840	121.314	16.75	5.02	-
97/01/05	10:34:18.63	24.670	122.320	5.00	5.52	5.2
97/01/16	01:07:20.32	22.007	121.306	6.55	5.26	-
97/03/24	23:32:19.97	24.157	121.725	31.13	5.09	-
97/05/03	02:46:14.56	22.520	121.364	8.50	5.39	5.0
97/06/22	09:36:04.34	22.157	121.390	4.57	5.37	5.2
97/07/04	18:37:29.68	23.059	120.792	1.83	5.11	5.1
97/10/22	11:16:26.28	22.409	121.490	13.82	5.36	-
97/11/14	04:29:51.14	24.176	121.732	3.37	5.29	-
98/01/18	19:56:51.53	22.761	121.009	6.97	5.17	5.2
98/03/11	17:21:54.84	22.443	122.261	4.07	5.25	-
98/07/17	04:51:15.02	23.503	120.664	5.71	5.90	5.7
98/07/24	18:44:02.57	21.602	121.839	5.39	6.03	6.1
98/10/09	12:52:51.65	22.196	121.584	1.40	5.53	-
98/11/03	07:06:37.43	22.132	121.127	25.04	5.28	-
98/11/17	22:27:31.84	22.828	120.793	27.01	5.65	5.3
98/12/14	00:59:03.50	24.290	122.157	34.22	5.10	-
99/06/10	07:17:59.88	23.797	121.558	32.06	5.06	-
99/07/07	13:53:12.86	23.305	120.757	18.88	5.10	-
99/09/20	17:47:15.85	23.853	120.815	8.00	7.06	7.6
99/09/20	17:57:15.46	23.923	121.038	5.93	6.05	-
99/09/20	18:03:42.05	23.806	120.850	9.97	6.26	-
99/09/20	18:11:52.00	23.899	121.031	5.29	6.35	-
99/09/20	18:16:17.31	23.866	121.059	8.36	6.33	-
99/09/20	21:46:36.86	23.564	120.904	4.39	6.22	6.4
99/09/22	00:14:40.77	23.826	121.047	15.59	6.47	6.4
99/09/22	00:49:42.39	23.746	121.006	6.03	5.97	5.8
99/09/22	11:17:20.94	23.718	121.003	18.06	5.54	5.2
99/09/23	12:44:33.83	23.910	121.082	19.71	5.36	5.2
99/09/25	08:43:28.92	23.642	120.978	7.38	5.43	5.1
99/09/25	23:52:47.28	23.826	120.994	20.90	6.44	6.5
99/10/01	12:54:09.35	23.684	120.943	8.00	5.26	5.2
99/10/04	12:26:12.60	23.788	120.955	11.24	5.01	-
99/10/18	16:00:39.56	23.714	121.061	25.42	5.32	5.3
99/10/22	02:18:56.55	23.496	120.422	23.14	6.07	5.8
99/10/22	03:10:16.35	23.505	120.436	19.78	5.86	5.5

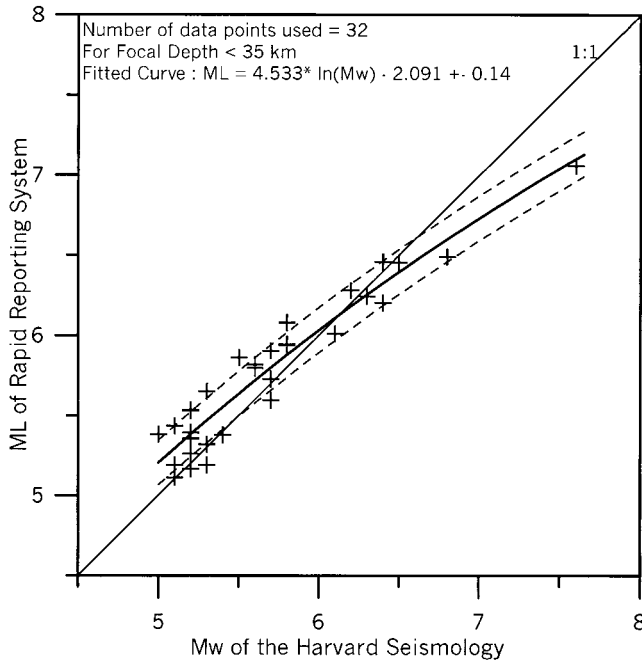


Figure 4. Relationship between M_w and M_L for shallow earthquakes in the Taiwan region.

mined by regression analysis. A relation between earthquake fault rupture area and magnitude can be expressed as (Wyss, 1979)

$$M = \log_{10}(A_{rup}) + C, \quad (3)$$

where M is magnitude, A_{rup} is fault rupture area in km^2 , and C is a constant. For the case of the Chi-Chi earthquake, M_w is 7.6, the fault area is $80 \times 40 \text{ km}^2$ (Kikuchi *et al.*, 2000), and then C can be determined to be 4.12, and h can be expressed as $0.00871 \times 10^{0.5M_w}$. This value is used in our regression calculations. A total of 1941 records are used in the regression process. Data selection criteria are as follows: (1) all of the T system records of the 60 events in Table 1, and (2) source-to-site distance less than 30 km for the TSMIP records of the 60 events in Table 1.

In the regression process we only used the source-to-site distance less than 30 km of the TSMIP records. The reasons are that recording is likely more complete in the near source areas because the TSMIP instruments are maintained in trigger mode. Thus, more distant instruments may not be triggered when seismic ground motion decays to below a trigger threshold. Only instruments in the large site amplification areas will be triggered. On the contrary, instruments in small site amplification areas will not be triggered. This phenomenon will cause over-estimated of the attenuation curve in more distant zones.

The resulting attenuation relationships for PGA and PGV are given by

$$\log_{10}(\text{PGA}) = 0.00215 + 0.581M_w - \log_{10}(r_{rup}) + 0.00871 \times 10^{0.5M_w} - 0.00414r_{rup} \quad (4)$$

$$\log_{10}(\text{PGV}) = -2.49 + 0.810M_w - \log_{10}(r_{rup}) + 0.00871 \times 10^{0.5M_w} - 0.00268r_{rup} \quad (5)$$

where the PGA unit is cm/sec^2 , the PGV unit is cm/sec , and r_{rup} is rupture distance in km. The comparisons between the observed and predicted PGA and PGV values are shown in Figures 5 and 6, respectively. The standard deviations of the residuals between the observed and predicted values (i.e., $\ln(\text{observed}) - \ln(\text{predicted})$) are 0.79 and 0.75 for PGA and PGV (Figs. 7, 8), respectively. According to the regression results, the PGV fit is better than that of the PGA. Generally, smaller earthquakes can produce high PGA in a near-source area, but they cannot produce high PGV in a near-source area. Obviously, a smaller earthquake in a near-source area with a high PGA is caused by a more higher-frequency signal than is a bigger earthquake. Thus, it does not produce high PGV in the near-source area. The attenuation relationships are determined for a magnitude range from M_w 4.8 to 7.6. Therefore, it is appropriate for damage assessment application in a rapid reporting system.

Estimating the TSMIP Site Ground Motions

The TSMIP stations cover almost all of the populated areas of the Taiwan. Therefore, estimating the TSMIP site ground motions will be very important for damage assessment. Generally, site effect is one of the important factors for predicting ground motion. The TSMIP sites still have not been well classified (Lee *et al.*, 2001). However, those stations have recorded many earthquakes. Thus, the TSMIP site correction, S , can be determined empirically by averaging the residuals between the observed and predicted values as following:

$$S = \exp\left(\frac{1}{n} \sum_{i=1}^n \ln(D_i/\bar{D}_i)\right), \quad (6)$$

where D_i is either the observed PGA or PGV value, and \bar{D}_i is either the predicted PGA or PGV value obtained by the attenuation relationships. Thus, the TSMIP site peak ground motion can be expressed as $S \times \bar{D}_i$. Figures 9 and 10 show the PGA and PGV site correction contour maps of the TSMIP stations. The results show that the western coastal plain, Taipei basin, and Pingtung and Lanyang plains are places of high amplification (Fig. 1). On the other hand, the Central Mountain Range and the eastern Taiwan areas are places of low amplification. The results agree reasonably well with the surface geology from published maps. After applying the site amplification correction in the regression process, the standard deviations of the residuals between the observed

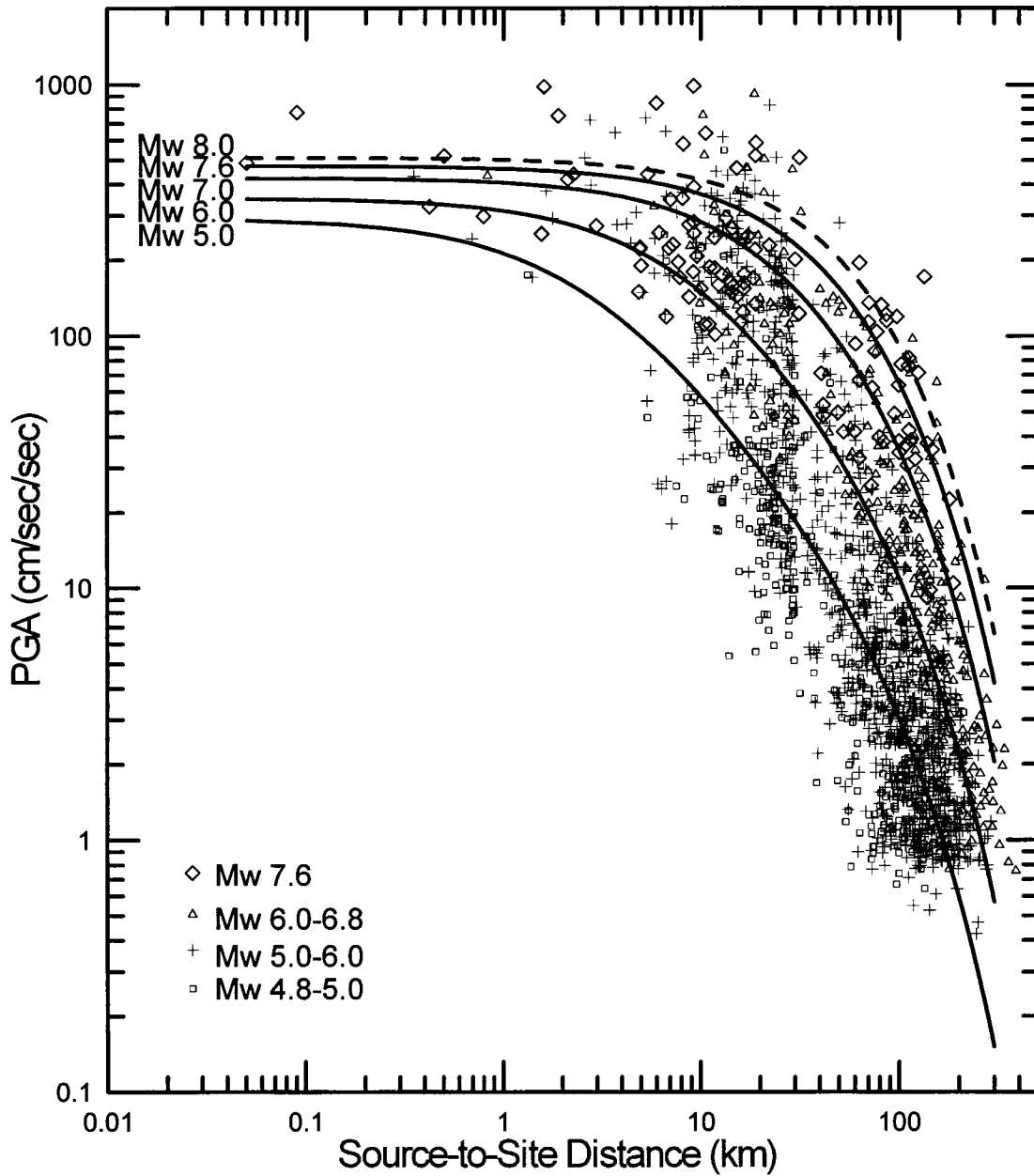


Figure 5. The 1941 observed PGAs and the predicted curves.

and predicted values significantly decreased to 0.66 and 0.61 for PGA and PGV (Figs. 7, 8), respectively.

Immediately after a strong earthquake, PGA and PGV values of all of the T system stations are available at the CWB headquarters. The peak ground motion P at a TSMIP site can be estimated by

$$P = \bar{D} \times S \times \frac{T_{\text{obs}}}{T_{\text{cal}}}, \quad (7)$$

where \bar{D} is either the predicted PGA or PGV value obtained by the attenuation relationships, T_{obs} is the observed value

at the nearest T system station, and T_{cal} is the predicted value by the attenuation relationships with site correction at that T system station. Generally, the attenuation relationships and site corrections represent a statistically averaged effect. Every event possesses its own characteristics, such as the source radiation patterns and directivity effect. And the T system observed values imply such characteristics. Since our primary objective is to estimate the TSMIP site ground motions within 2 min after occurrence of a felt earthquake in the Taiwan region (Wu *et al.*, 2000), the procedure presented in this article represents a first-order measure of ground-motion intensity.

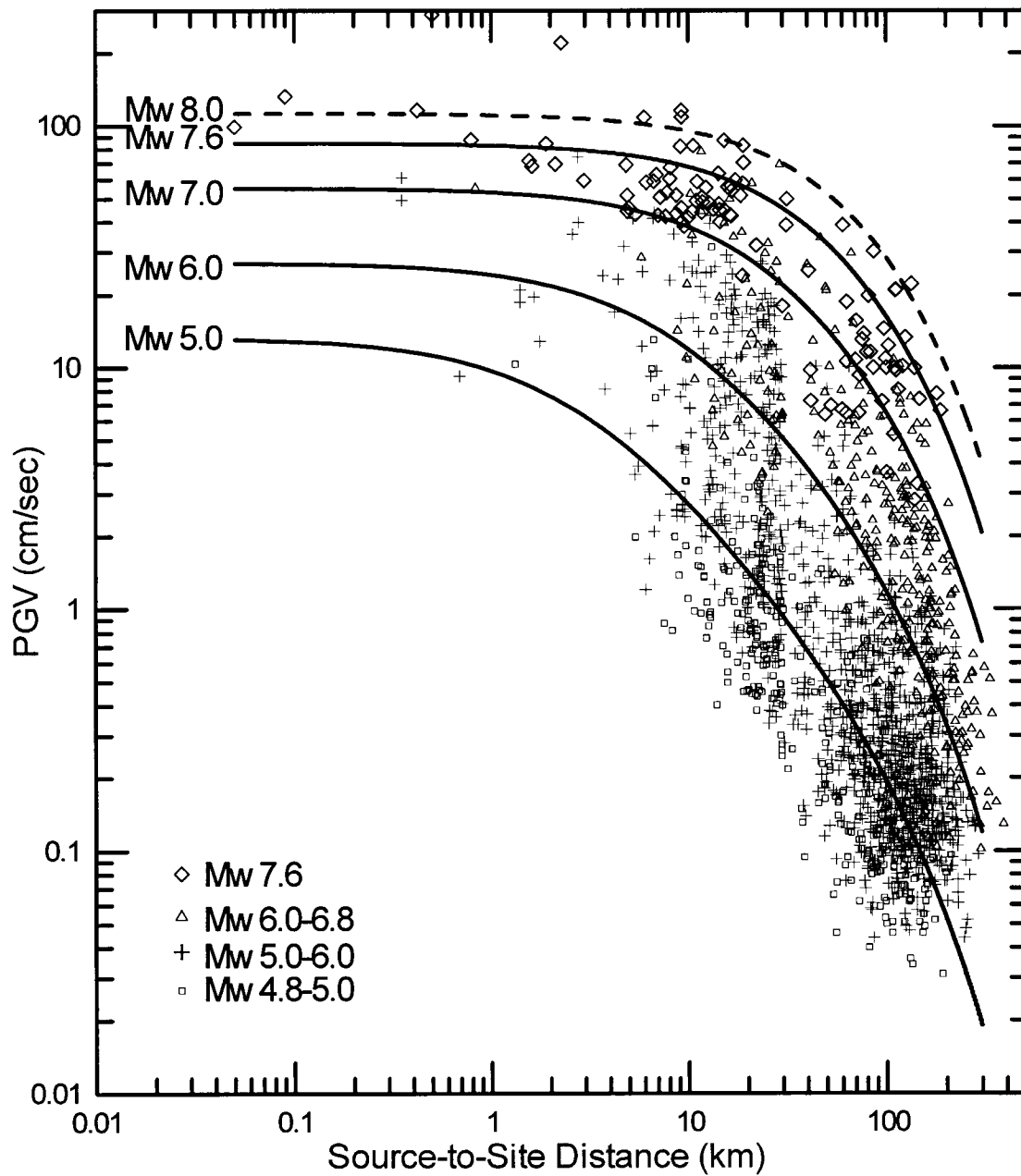


Figure 6. The 1941 observed PGVs and the predicted curves.

Validation Tests on Estimation of Peak Values

We use the extensive recordings of the Chi-Chi earthquake to test the estimation scheme outlined above. Figure 11D gives the reality—the PGA map based on both the T system and the TSMIP observations. If only the T system data are used, we have a PGA map that gives the basic and rough structure of Figure 11D. If only the calculated TSMIP PGA values are used, Figure 11B gives an inferior PGA map because the attenuation relationship is mainly based on a point source that deviates from the reality of the long Chi-Chi earthquake rupture. Figure 11C shows the result of the

estimation scheme outlined above, it gives a PGA map much more close to the observed PGA map given by Figure 11D. We conclude that our schemes are satisfactory in estimating the PGA values. However, Figure 9C still underestimates the PGA values to the north of the epicenter where the Che-lungpu rupture is terminating. This discrepancy mainly comes from insufficient source correction. However, the results are acceptable as first cut for practical applications.

Figure 12A and B shows the Chi-Chi mainshock distribution of the calculated and observed PGV values, respectively, at the TSMIP sites. Generally, the fitting is reasonably close except for a special high PGV area toward the north of

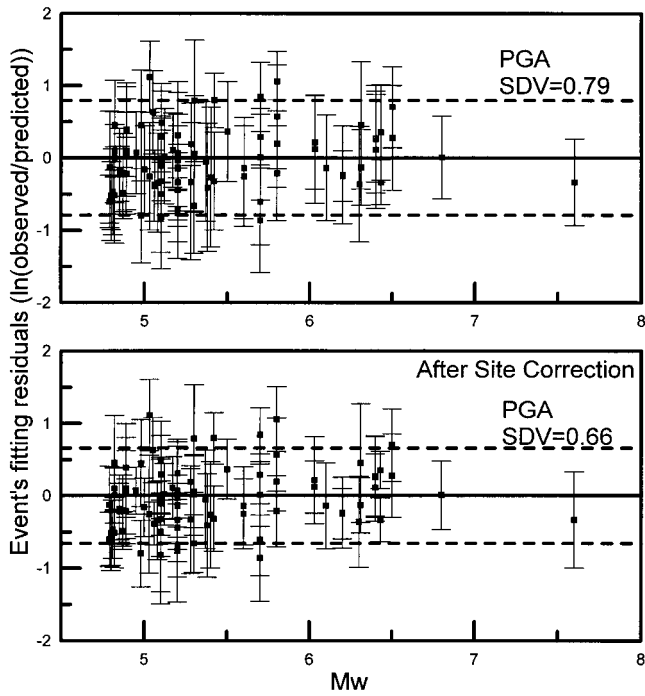


Figure 7. PGA residuals between the observed and predicted values in the regression process.

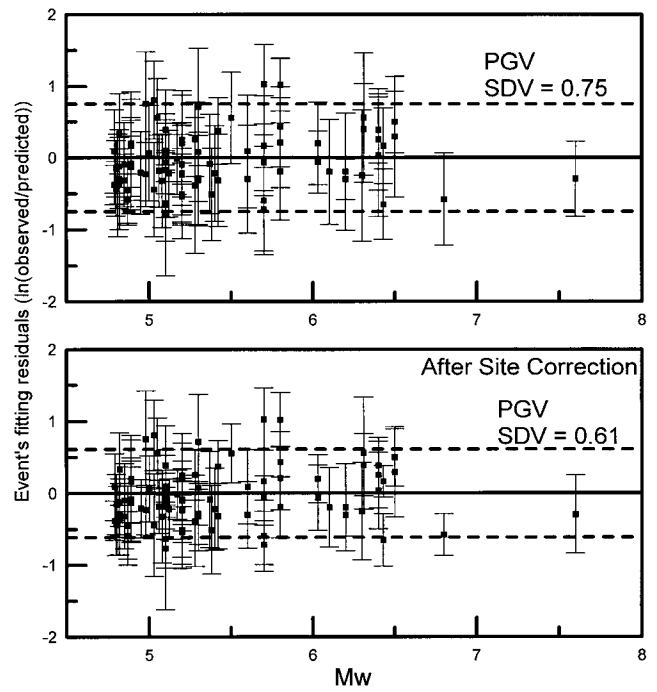


Figure 8. PGV residuals between the observed and predicted values in the regression process.

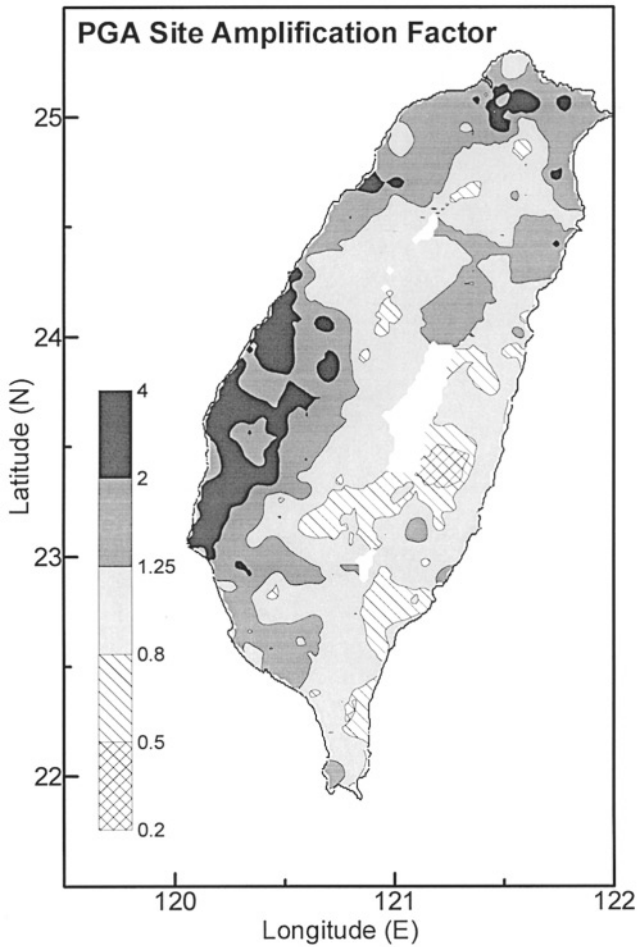


Figure 9. The PGA site correction factor contour map of the TSMIP stations.

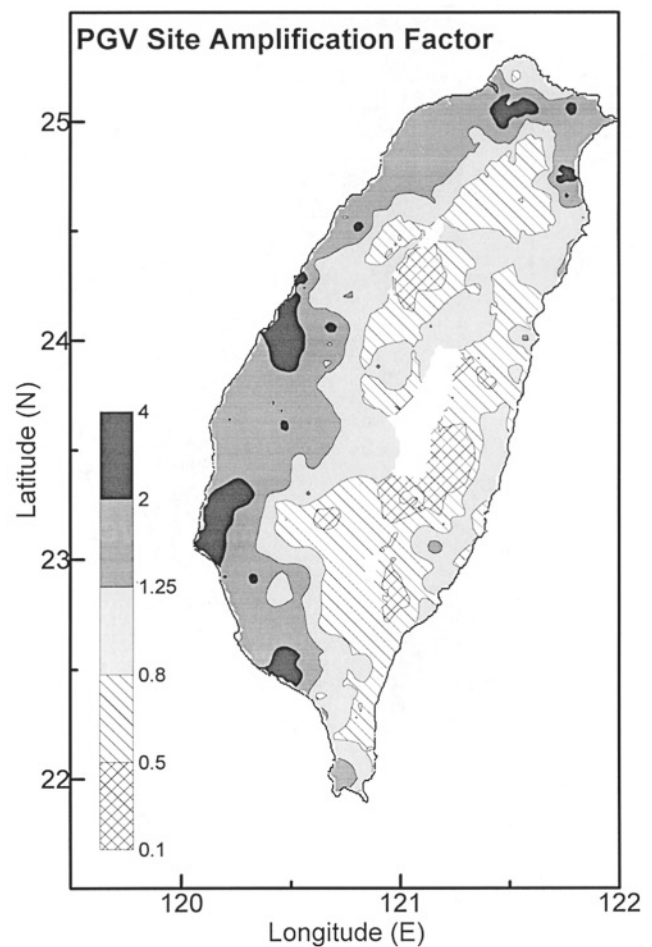


Figure 10. The PGV site correction factor contour map of the TSMIP stations.

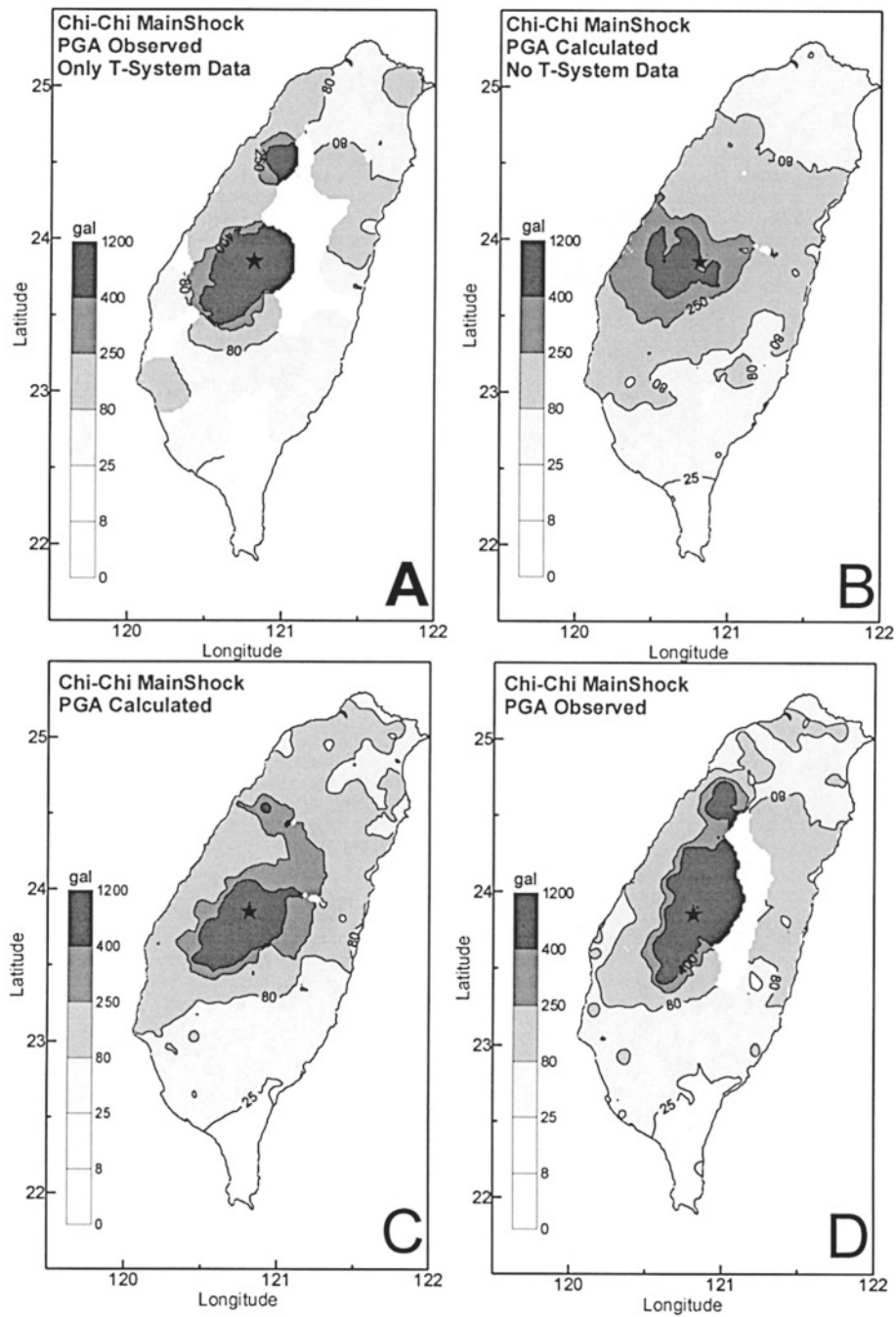


Figure 11. Maps A, B, C, and D show the Chi-Chi mainshock PGA distribution from the T system records, the predicted values from point source without the T system records, the predicted values, and the observed values, respectively.

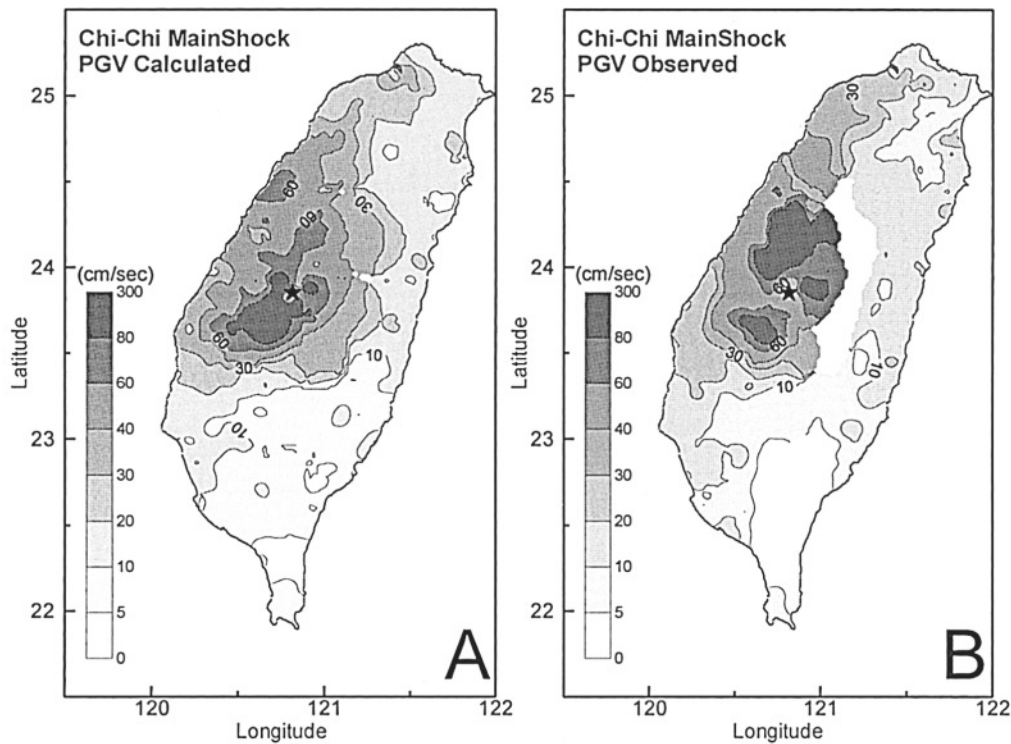


Figure 12. Maps A and B show the Chi-Chi mainshock PGA distribution of the predicted values and observed values, respectively.

the epicenter. This discrepancy again can be attributed to extensive length of the Chelungpu rupture and insufficient site corrections. However, the principal features in Figure 12A are not too far off for emergency response purpose. We have performed a similar validation test using data from a large (M_w 6.5) Chi-Chi aftershock that occurred on 25 September 1999. The calculated and observed PGA values are given in Figure 13A and B, respectively. The calculated and observed PGV values are given in Figure 13C and D. For events without extended rupture, the calculated peak values more closely approximate the observations.

Conclusions

From a large set of strong-motion data of 60 shallow large earthquakes recorded over a relatively short period of time (5 yr), we have derived the PGA and PGV attenuation relationships for shallow earthquakes in the Taiwan region. Using these attenuation relationships and the large amount of strong-motion data, especially from those densely distributed 650 or so TSMIP stations, we have derived the site effect corrections for all strong-motion station sites in Taiwan. With the attenuation relationships and the site corrections database, we have developed and tested a practical procedure for the calculating PGA and PGV values as soon as (in 2 min) a strong earthquake happens in Taiwan. The only input this peak values calculation procedure needs is the T-system so-

lution (that can provide the earthquake location and magnitude in 1 min). This will be incorporated into the current CWB seismic network operation. We expect that the calculated PGA and PGV maps will be useful for earthquake emergency response operations.

Acknowledgments

We wish to thank Prof. Ta-liang Teng and Prof. Yi-Ben Tsai for greatly improving this article and providing many thought-provoking comments. We also wish to thank Dr. Lupei Zhu for reviewing and greatly improving this article. This research was supported by the National Science Council of the Republic of China under Grant No. NSC89-2625-Z-052-023.

References

- Espinosa-Aranda, J., A. Jiménez, G. Ibarrola, F. Alcantar, A. Aguilar, M. Inostroza, and S. Maldonado (1995). Mexico City seismic alert system, *Seism. Res. Lett.* **66**, 42–53.
- Gee, L. S., D. S. Neuhauser, D. S. Dreger, M. E. Pasyanos, R. A. Uhrhammer, and B. Romanowicz (1996). Real-time seismology at UC Berkeley: The Rapid Earthquake Data Integration Project, *Bull. Seism. Soc. Am.* **86**, 936–945.
- Heaton, T. H. (1985). A model for a seismic computerized alert network, *Science* **228**, 987–990.
- Kanamori, H., E. Hauksson, and T. Heaton (1997). Real-time seismology and earthquake hazard mitigation, *Nature* **390**, 461–464.

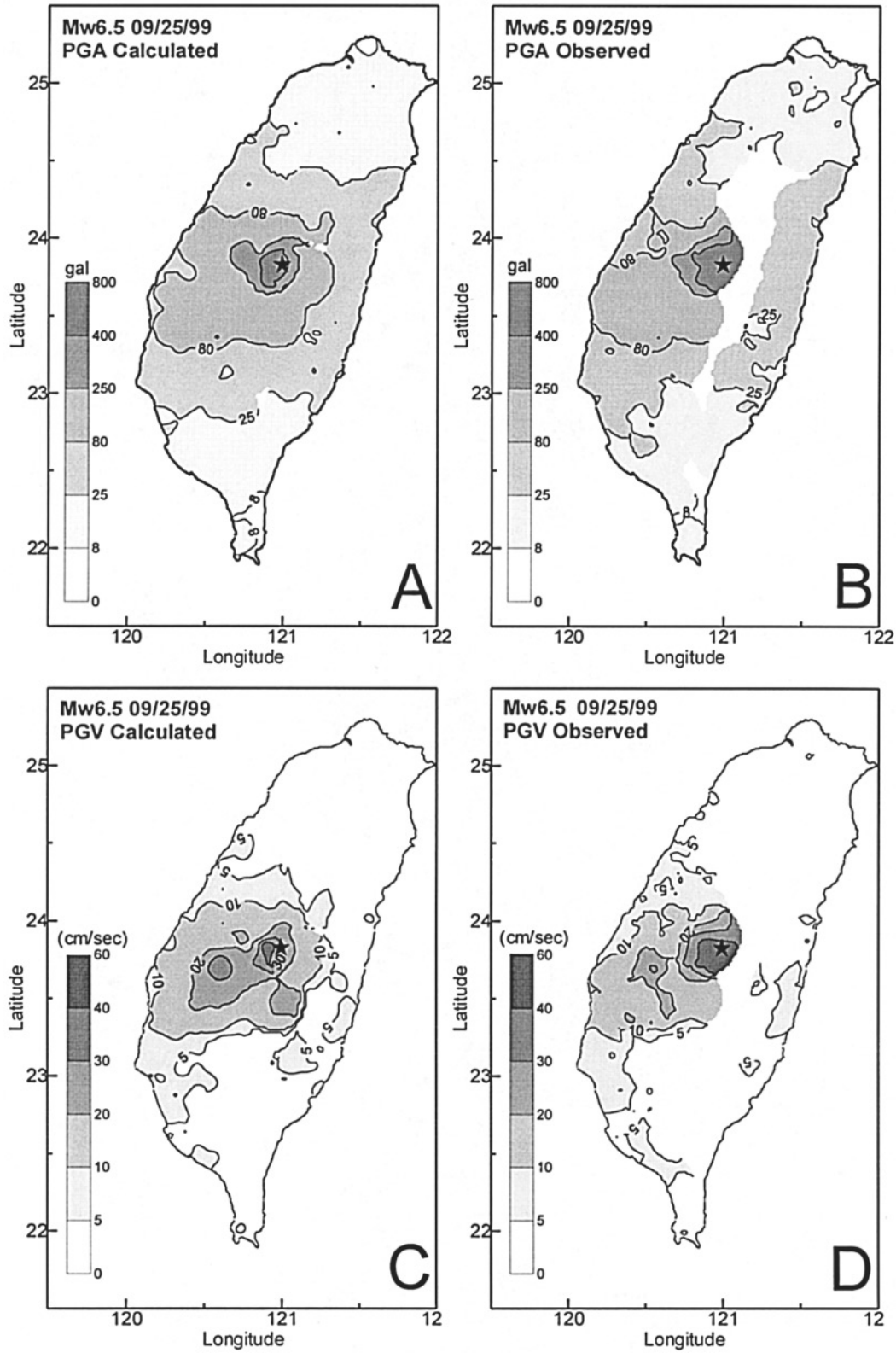


Figure 13. Maps A, B, C, and D show a Chi-Chi aftershock (25 September 1999) (M_w 6.5) predicted and observed PGA distribution, and predicted and observed PGV distribution, respectively.

- Kikuchi, M., Y. Yagi, and Y. Yamanaka (2000). Source process of the Chi-Chi, Taiwan earthquake of September 21, 1999 inferred from teleseismic body waves, *Bull. Earthquake Res. Inst. Univ. Tokyo* **75**, 1–13.
- Lee, C. T., C. T. Cheng, C. W. Liao, and Y. B. Tsai (2001). Site classification of Taiwan free-field strong motion stations, *Bull. Seism. Soc. Am.* (submitted).
- Liu, K. S. (1999). Attenuation relationships for strong ground motion in Taiwan, *Ph. D. Dissertation*, Institute of Geophysics, National Central University, Chung-Li, Taiwan, 240 pp.
- Nakamura, Y. (1988). On the urgent earthquake detection and alarm system (UrEDAS), in Proc. of the 9th World Conference on Earthquake Engineering, Tokyo-Kyoto, 2–9 August, Japan.
- Nakamura, Y. (1989). Earthquake alarm system for Japan railways, *Japanese Railway Engineering* **109**, 1–7.
- Shin, T. C. (1993). The calculation of local magnitude from the simulated Wood-Anderson seismograms of the short-period seismograms, *TAO* **4**, 155–170.
- Shin, T. C., K. W. Kuo, W. H. K. Lee, T. L. Teng, and Y. B. Tsai (2000). A preliminary report on the 1999 Chi-Chi (Taiwan) earthquake, *Seism. Res. Lett.* **71**, 24–30.
- Teng, T. L., L. Wu, T. C. Shin, Y. B. Tsai, and W. H. K. Lee (1997). One minute after: strong-motion map, effective epicenter, and effective magnitude, *Bull. Seism. Soc. Am.* **87**, 1209–1219.
- Wald, D. J., V. Quitoriano, L. Dengler, and J. W. Dewey (1999). Utilization of the internet for rapid community seismic intensity maps, *Seism. Res. Lett.* **70**, 680–693.
- Wald, D. J., V. Quitoriano, T. H. Heaton, H. Kanamori, C. W. Scrivner, and C. B. Worden (1999b). TriNet “ShakeMaps”: rapid generation of instrumental ground motion and intensity maps for earthquakes in Southern California, *Earthquake Spectra* **15**, 537–556.
- Wu, Y. M., T. C. Shin, and Y. B. Tsai (1998). Quick and reliable determination of magnitude for seismic early warning, *Bull. Seism. Soc. Am.* **88**, 1254–1259.
- Wu, Y. M., C. C. Chen, T. C. Shin, Y. B. Tsai, W. H. K. Lee, and T. L. Teng (1997). Taiwan Rapid Earthquake Information Release System, *Seism. Res. Lett.* **68**, 931–943.
- Wu, Y. M., J. K. Chung, T. C. Shin, N. C. Hsiao, Y. B. Tsai, W. H. K. Lee, and T. L. Teng (1999). Development of an integrated seismic early warning system in Taiwan, *TAO* **10**, 719–736.
- Wu, Y. M., W. H. K. Lee, C. C. Chen, T. C. Shin, T. L. Teng, and Y. B. Tsai (2000). Performance of the Taiwan Rapid Earthquake Information Release System (RTD) during the 1999 Chi-Chi (Taiwan) earthquake, *Seism. Res. Lett.* **71**, 328–333.
- Wyss, M. (1979). Estimating maximum expectable magnitude of earthquakes from fault dimensions, *Geology* **7**, 336–340.

Central Weather Bureau
Taipei, Taiwan, R.O.C.

Manuscript received 1 December 2000.